the plant journal

SEB SOCIETY FOR EXPERIMENTAL BIOLOGY

The Plant Journal (2021) doi: 10.1111/tpj.15300

Crystal structure of chloroplastic thioredoxin z defines a type-specific target recognition

Théo Le Moigne[1,2,3], Libero Gurrieri[4], Pierre Crozet[1,3,5], Christophe H. Marchand[1,3,6], Mirko Zaffagnini[4], Francesca Sparla[4], Stéphane D. Lemaire[1,3] and Julien Henri[1,3,*]

[1]*Laboratoire de Biologie Computationnelle et Quantitative, Institut de Biologie Paris-Seine, UMR 7238, CNRS, Sorbonne Université, 4 Place Jussieu, Paris 75005, France,*

[2]*Faculty of Sciences, Doctoral School of Plant Sciences, Université Paris-Saclay, Saint-Aubin 91190, France,*

[3]*Laboratoire de Biologie Moléculaire et Cellulaire des Eucaryotes, Institut de Biologie Physico-Chimique, UMR 8226, CNRS, Sorbonne Université, 13 Rue Pierre et Marie Curie, Paris 75005, France,*

[4]*Department of Pharmacy and Biotechnology, University of Bologna, Via Irnerio 42, Bologna 40126, Italy,*

[5]*Sorbonne Université, Polytech Sorbonne, Paris 75005, France, and*

[6]*Plateforme de Protéomique, Institut de Biologie Physico-Chimique, FR 550, CNRS, 13 Rue Pierre et Marie Curie, Paris 75005, France*

Received 18 December 2020; revised 13 April 2021; accepted 22 April 2021.
*For correspondence (e-mail julien.henri@sorbonne-universite.fr).

SUMMARY

Thioredoxins (TRXs) are ubiquitous disulfide oxidoreductases structured according to a highly conserved fold. TRXs are involved in a myriad of different processes through a common chemical mechanism. Plant TRXs evolved into seven types with diverse subcellular localization and distinct protein target selectivity. Five TRX types coexist in the chloroplast, with yet scarcely described specificities. We solved the crystal structure of a chloroplastic z-type TRX, revealing a conserved TRX fold with an original electrostatic surface potential surrounding the redox site. This recognition surface is distinct from all other known TRX types from plant and non-plant sources and is exclusively conserved in plant z-type TRXs. We show that this electronegative surface endows thioredoxin z (TRXz) with a capacity to activate the photosynthetic Calvin–Benson cycle enzyme phosphoribulokinase. The distinct electronegative surface of TRXz thereby extends the repertoire of TRX–target recognitions.

Keywords: Calvin–Benson cycle, Photosynthesis, protein structure, protein–protein interactions, redox post-translational modifications, thioredoxins.

INTRODUCTION

Thioredoxins (TRXs) are small ubiquitous disulfide oxidoreductases (Buchanan *et al.*, 2012; Gleason and Holmgren, 1981; Hall *et al.*, 1971; Holmgren, 1968; Lillig and Holmgren, 2007). TRXs fold into a highly conserved and thermostable domain composed of a mixed β-sheet closely surrounded by α-helices and exposing a WC(G/P)PC pentapeptidic motif (Holmgren, 1968; Pan and Bardwell, 2006). Phylogenetic analyses described the history of the TRX fold through 4 billion years of evolution into the contemporary proteins (Ingles-Prieto *et al.*, 2013; Napolitano *et al.*, 2019). TRXs modify the ternary or quaternary structures of proteins by reducing target disulfide bonds into separate thiols (Blomback *et al.*, 1974; Holmgren and Morgan, 1976). TRXs have also been proposed to be involved in other redox modifications of cysteines by catalyzing denitrosylation, deglutathionylation, or depersulfidation reactions, contributing therefore to redox signaling cascades and metabolic remodeling (Bedhomme *et al.*, 2012; Benhar *et al.*, 2008; Berger *et al.*, 2016; Greetham *et al.*, 2010; Wedmann *et al.*, 2016), as recently reviewed in Zaffagnini *et al.* (2016, 2019). The midpoint redox potential of TRXs lies between −310 and −230 mV at pH 7 (Collin *et al.*, 2003; Gonzalez Porque *et al.*, 1970; Hirasawa *et al.*, 1999; Setterdahl *et al.*, 2003; Watson *et al.*, 2003) with a nucleophilic active site cysteine reacting in the thiolate state ($-S^-$), favored at physiological pH by a local environment determining a cysteine pK_a in the 6.5–7.5 range (Ferrer-Sueta *et al.*, 2011; Marchand *et al.*, 2019; Roos *et al.*, 2013).

The TRX system is recognized as having multiple roles in a myriad of cellular processes and numerous human

© 2021 Society for Experimental Biology and John Wiley & Sons Ltd

diseases (Buchanan *et al.*, 2012; Hanschmann *et al.*, 2013; Lee *et al.*, 2013; Toledano *et al.*, 2013). Non-photosynthetic organisms contain a limited number of TRXs reduced by NADPH:thioredoxin reductase (NTR). By contrast, TRXs are encoded by a larger multigene family in photosynthetic organisms (21 isoforms in the model plant *Arabidopsis thaliana* and 10 in the unicellular green alga *Chlamydomonas reinhardtii*). Phylogenetic analyses grouped TRXs in the cytosolic/mitochondrial h-type, the mitochondrial o-type, and five chloroplastic types (f-, m-, x-, y-, and z-types) (Balsera *et al.*, 2014; Michelet *et al.*, 2006). Cytosolic and mitochondrial TRXs are reduced by NTR but chloroplastic TRXs are specifically reduced in the light by ferredoxin: thioredoxin reductase (FTR), which derives electrons from ferredoxin and the photosynthetic electron transfer chain (Balsera *et al.*, 2014; Jacquot *et al.*, 2009; Kang *et al.*, 2019; Michelet *et al.*, 2013; Schurmann and Buchanan, 2008; Zaffagnini *et al.*, 2019). This unique reduction mechanism allows to couple the redox state of TRX to light intensity and to use the chloroplast TRX system as a light-dependent signaling pathway for regulation of cellular metabolism and processes (Perez-Perez *et al.*, 2017). In photoautotrophic organisms, TRXs were originally identified as light-dependent regulators of the Calvin–Benson cycle (CBC), responsible for fixation of atmospheric CO_2 into triose phosphates using energy (ATP) and reducing power (NADPH) produced in the light by the photosynthetic electron transfer chain. Early studies identified four key enzymes of the CBC as TRX targets: phosphoribulokinase (PRK) (Wolosiuk and Buchanan, 1978b), glyceraldehyde-3-phosphate dehydrogenase (GAPDH) (Wolosiuk and Buchanan, 1978a), fructose-1,6-bisphosphatase (FBPase) (Holmgren *et al.*, 1977), and sedoheptulose-1,7-bisphosphatase (SBPase) (Nishizawa and Buchanan, 1981). These enzymes have a low activity in the dark and are activated upon illumination by the ferredoxin/TRX system because reduction of specific regulatory disulfides by TRX triggers conformational changes that shift the enzyme to a high-activity conformation. Besides the CBC, chloroplast TRXs were later recognized as regulators of multiple targets involved in numerous pathways and processes (Lemaire *et al.*, 2007; Zaffagnini *et al.*, 2019). TRXs were especially recognized to provide electrons for the regeneration of major antioxidant enzymes such as peroxiredoxins (Collin *et al.*, 2003; Liebthal *et al.*, 2018; Navrot *et al.*, 2006; Perez-Perez *et al.*, 2009; Sevilla *et al.*, 2015; Tarrago *et al.*, 2009; Yoshida *et al.*, 2019b).

In the microalga *C. reinhardtii*, 10 TRX isoforms have been identified, including six nuclear-encoded chloroplastic TRXs (CrTRXf1, CrTRXf2, CrTRXm, CrTRXx, CrTRXy, and CrTRXz) (Balsera *et al.*, 2014; Lemaire *et al.*, 2007; Zaffagnini *et al.*, 2019). Proteomic analyses based on affinity purification chromatography and *in vitro* reconstitution of the cytosolic TRX system allowed the identification of 1053 TRX targets and 1052 putative regulatory sites in *Chlamydomonas* (Lemaire *et al.*, 2004; Perez-Perez *et al.*, 2017). Among these, all CBC enzymes were identified, indicating that they are potential TRX interactors, and direct TRX-dependent activation of CBC enzymes was only demonstrated for PRK (Gurrieri *et al.*, 2019), FBPase (Huppe and Buchanan, 1989), SBPase (Gutle *et al.*, 2016), and phosphoglycerate kinase (PGK) (Morisse *et al.*, 2014). By contrast with land plants, photosynthetic GAPDH from *C. reinhardtii* (CrGAPDH) is not directly regulated by TRX but only indirectly through formation of the $(A_4\text{-GAPDH})_2$–$CP12_4$–PRK_2 complex (Avilan *et al.*, 2012; Marri *et al.*, 2009; Trost *et al.*, 2006). Among the five TRX types present in chloroplasts, only TRXf has been systematically compared to other types and demonstrated to target FBPase (Collin *et al.*, 2003; Michelet *et al.*, 2013), PRK (Gurrieri *et al.*, 2019; Marri *et al.*, 2009), GAPDH in land plants (Marri *et al.*, 2009), and PGK in *Chlamydomonas* (Morisse *et al.*, 2014). Structural analysis revealed that electrostatic complementarity is the principal driver of TRXf–target recognition (Balmer *et al.*, 2004; Bunik *et al.*, 1999; De Lamotte-Guery *et al.*, 1991; Lemaire *et al.*, 2018; Mora-Garcia *et al.*, 1998). Besides, TRXs were recently attributed a reciprocal redox function for the oxidation of targets upon light-to-dark transitions through the action of TRXL2 and 2-Cys peroxiredoxins (Cejudo *et al.*, 2019; Ojeda *et al.*, 2018; Vaseghi *et al.*, 2018; Yoshida *et al.*, 2018, 2019a, 2019b). Finally, TRXs are involved in a multiplicity of other plastid functions either through their redox capacities (Kang *et al.*, 2019), in the complex redox cellular network (Konig *et al.*, 2012; Yoshida and Hisabori, 2016), or through participation in large supramolecular assemblies (Kulczyk *et al.*, 2017; Schroter *et al.*, 2010).

In *Populus trichocarpa* and in *A. thaliana*, TRXz was reported to be reduced by FTR (Chibani *et al.*, 2011; Yoshida and Hisabori, 2017). TRXz can also act as a potential electron acceptor for a special type of chloroplastic TRX named NADPH:thioredoxin reductase C (NTRC) (Yoshida and Hisabori, 2016), TRXf, m, x, and y (Bohrer *et al.*, 2012), and interacts with fructokinase-like proteins (FLN1 and FLN2) in *A. thaliana* and *Nicotiana benthamiana* (Arsova *et al.*, 2010). TRXz–FLN interaction regulates plastid-encoded polymerase (PEP) (Arsova *et al.*, 2010; Huang *et al.*, 2013). Notably, TRXz reduces plastid redox-insensitive protein 2 (PRIN2) cysteine 68 (C68) heteromolecular disulfides bridges within a homodimer in *A. thaliana*, releasing monomeric PRIN2, which activates PEP transcription (Diaz *et al.*, 2018). TRXz redox activity may however be dispensable and TRXz–FLN1 are proposed to be essential components of the PEP complex (Wimmelbacher and Bornke, 2014). TRXz also interacts with *A. thaliana* thioredoxin-like MRL7 (Yua *et al.*, 2014) and temperature-sensitive virescent protein mediates the TRXz interaction with PEP in rice (*Oryza sativa*) (Sun *et al.*, 2017). In rice, TRXz was also found to interact with chloroplastic

© 2021 Society for Experimental Biology and John Wiley & Sons Ltd,

RNA-editing enzymes (Wang *et al.*, 2020). Yet, the full set of TRXz targets or interaction partners has not yet been elucidated and the corresponding molecular basis for TRXz specificity towards its targets remains to be deciphered.

Altogether, it is striking that the very ancient and simple 12–15-kDa TRX fold has evolved into this plethora of functions, suggesting a fine selection of redox properties and specific surface recognitions. In order to gain insights into the molecular functions of chloroplastic z-type TRXz and the physico-chemical basis for its specificity, we solved the high-resolution crystal structure of TRXz from *C. reinhardtii*. This structure is representative of a z-type TRX and unravels a conserved native folding compared to other structurally solved TRXs. Model analysis mapped its redox site and identified the surfaces it exposes for selective protein recognition. TRXz displays electro-complementary surfaces with *C. reinhardtii* PRK (CrPRK). We show that PRK is indeed activated by TRXz reduction *in vitro*.

RESULTS

CrTRXz folds as a canonical TRX

Recombinant TRXz from *C. reinhardtii* (CrTRXz) was heterologously expressed in *Escherichia coli* as a 149-amino acid polypeptide (predicted mature protein including residues 56–183 plus the N-terminal affinity tag) and purified to homogeneity by metal-affinity chromatography. Purified CrTRXz was crystallized, and the crystals were cryoprotected, submitted to X-ray diffraction for the collection of a complete dataset indexed in space group $P3_221$, and solved by molecular replacement with CrTRXf2 (Protein Data Bank [PDB] ID: 6I1C) as a search model. Model correction and completion up to 116 amino acid residues and one water molecule was refined to $R = 0.2296$ and $R_{free} = 0.2335$ at a resolution of 2.4 Å (Table 1). CrTRXz folds according to the canonical TRX topology (SCOPe entry c.47), that is, a central mixed β-sheet of four strands sandwiched between two pairs of α-helices (Figure 1(a,b)). The strand order is 2–1–3–4, with strand 3 antiparallel to strands 1, 2, and 4. The succession of secondary structures is as follows: residues 67–76 form helix 1, residues 80–86 strand 1, residues 91–107 helix 2, residues 111–117 strand 2, residues 122–128 helix 3, residues 135–139 strand 3, residues 148–151 strand 4, and residues 156–167 helix 4 (Figure S1). The length of helix 1 is conserved in the eukaryotic branch of TRX evolution since the last eukaryotic common ancestor (Ingles-Prieto *et al.*, 2013). Residues 118–120 were modeled as one turn of a helix 3_{10} with D119 hydrogen-bonding with W89 and the unique water molecule of the model. Residues ^{54}HMVI^{57} and ^{61}KVEKIS^{66} of recombinant CrTRXz form an unfolded extension at the N-terminus of the model, deforming it from an ideal sphere. Residues 58–60 and 170–183 were not built because of a lack of interpretable electron density. Pairwise alignments of equivalent C_α of CrTRXf2 and CrTRXm onto CrTRXz yielded a root mean square deviation (RMSD) of 0.838 Å and 1.356 Å, respectively, confirming the close structural similarity between the experimentally solved *Chlamydomonas* TRX structures (Figure S2). Further alignments with experimentally determined structures from the PDB revealed also high similarities with *Plasmodium falciparum* TRX2 (PDB ID: 3UL3, RMSD = 1.16 Å), resurrected ancestral TRX from the inferred last bacterial common ancestor (PDB ID: 4BA7, RMSD = 1.18 Å), *Bacteroides fragilis* TRXP (PDB ID: 3HXS, RMSD = 1.19 Å), and 20 other TRXs with RMSD ≤ 1.30 Å. CrTRXz topology is classical among TRXs.

CrTRXz redox site and environment

Disulfide oxidoreductase activity of TRX relies on a pair of cysteines located at the N-terminal tip of helix 2 in a conserved motif composed of the WCGPC peptide. The

Table 1 Crystallographic diffraction data and model statistics

	CrTRXz
Resolution range	40.34–2.444 (2.532–2.444)
Space group	P 32 2 1
Unit cell	61.985 61.985 61.138 90 90 120
Total reflections	210 020 (19 582)
Unique reflections	5300 (485)
Multiplicity	39.6 (38.0)
Completeness (%)	99.40 (94.17)
Mean I/sigma (I)	17.68 (1.29)
Wilson B-factor	65.65
R-merge	0.6065 (1.461)
R-meas	0.6145 (1.48)
R-pim	0.09769 (0.2389)
CC1/2	0.909 (0.792)
CC*	0.976 (0.94)
Reflections used in refinement	5269 (485)
Reflections used for R-free	525 (36)
R-work	0.2296 (0.3471)
R-free	0.2335 (0.3213)
CC (work)	0.462 (0.009)
CC (free)	0.38 (0.246)
Number of non-hydrogen atoms	865
Macromolecules	864
Solvent	1
Protein residues	113
RMS (bonds)	0.010
RMS (angles)	1.44
Ramachandran favored (%)	99.08
Ramachandran allowed (%)	0.92
Ramachandran outliers (%)	0.00
Rotamer outliers (%)	7.37
Clashscore	6.82
Average B-factor	70.15
Macromolecules	70.19
Solvent	30

Statistics for the highest-resolution shell are reported in parentheses.
RMS, root mean square; TRXz, thioredoxin z.

© 2021 Society for Experimental Biology and John Wiley & Sons Ltd,

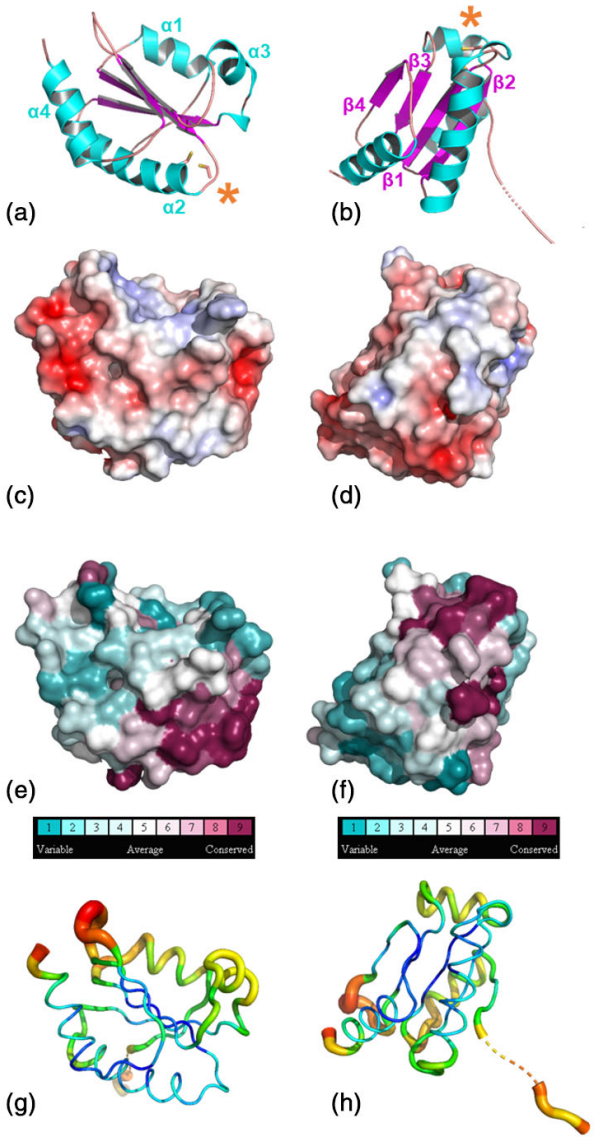

Figure 1. Crystallographic structure of chloroplastic CrTRXz.
(a) Cartoon representation with helices 1–4 colored in cyan and strands 1–4 colored in magenta. Cysteine side chains are represented in sticks and highlighted with an asterisk. Residue numbering is in accordance with UniProt entry A8J0Q8-1.
(b) 90° rotation around the *y*-axis of (a).
(c) Electrostatic surface potential calculated with APBS (Baker *et al.*, 2001). Electronegative surface is colored in red while electropositive surface is colored in blue.
(d) 90° rotation around the *y*-axis of (c).
(e) Conservation of surface residues as calculated with CONSURF colored from purple (most conserved) to blue (least conserved).
(f) 90° rotation around the *y*-axis of (e).
(g) B-factor representation. High B-factors are colored in red and low B-factors are colored in blue. APBS, Adaptive Poisson-Boltzman Solver; TRXz, thioredoxin z.

N-terminal active site cysteine (Cys_N) attacks the disulfide bond on a target protein while the second active site cysteine (Cys_C) resolves the intermolecular disulfide bridge to free the reduced target protein and the oxidized TRX. The mature CrTRXz sequence possesses two cysteines: Cys_N (C90) and Cys_C (C93) (Figure S1). Both are located at the tip of helix 2 (Figure 2(a)). Side chain thiols are modeled at 3.1 Å distance in what appears as a reduced state. The nucleophilic C90 displays a 13.56-$Å^2$ solvent-accessible area, making it available for redox exchange with a target protein disulfide. The orientation of its thiol group is however unfavorable to thiol electron exchange because it points inwards in the direction of the TRX core. A local rearrangement of loop 88–91 would be required to tumble the C90 thiol towards the solvent. Such a local rearrangement of the TRX redox site would partly account for the entropy dependence of target disulfide binding (Palde and Carroll, 2015). In *E. coli* TRX, D26 is buried in the core of the protein, where it acts as a base catalyst in the thiol–disulfide interchange reaction (Chivers and Raines, 1997; LeMaster *et al.*, 1997). D31 was confirmed to play the same role in CrTRXh1, and this requires a water molecule for proton exchange (Menchise *et al.*, 2001). CrTRXz also buries D84 at the equivalent position and its carboxyl side chain points in the direction of resolving C93 at a distance of 6.4 Å (Figure 2(b)). An intermediate water molecule, though not visible at the resolution of our structure, would fit in between at distances favoring hydrogen bonds with D84 and C93 (Figure 2(b)). P134 at the N-terminal side of strand 3 faces the redox site at 3.5 Å and 4.6 Å from C93 and C90, respectively. P134 is built in the *cis* conformation. As reported earlier, this *cis*-proline is an important kinetic bottleneck for protein folding (Kelley and Richards, 1987) and is already observed in inferred pre-Cambrian TRXs (Gamiz-Arco *et al.*, 2019). Altogether, the redox site microenvironment and structural-dependent functional features of TRXs are present and canonical in CrTRXz.

CrTRXz is monomeric

We unexpectedly observed early elution of purified CrTRXz during size-exclusion chromatography (SEC), showing an apparent higher molecular weight of the protein when compared to CrTRXf2. The experiment was repeated over two analytical gel filtration matrices (BioSEC3-300 and S6Increase) and the results were confirmed by comparison of distribution coefficients (Kav): $Kav(CrTRXz)_{BioSEC3\text{-}300} = 0.625 \pm 0.005$, $Kav(CrTRXf2)_{BioSEC3\text{-}300} = 0.89$; and $Kav(CrTRXz)_{S6Increase} = 0.611$, $Kav(CrTRXf2)_{S6Increase} = 0.723$ (Figure S3). According to BioSEC3-300 gel filtration calibrated with globular standards, the apparent molecular weight of CrTRXz is 30 ± 5 kDa, approximating twice the molecular weight of a 16-kDa subunit. Consequently, CrTRXz appears as a possible globular homodimer according to SEC analysis.

Analysis of protein interfaces in the crystal packing with PISA (EMBL-EBI) indeed uncovers six direct contact surfaces of 22.4, 98.9, 286.5, 322.1, 437.3, and 812.1 $Å^2$ of the

© 2021 Society for Experimental Biology and John Wiley & Sons Ltd,

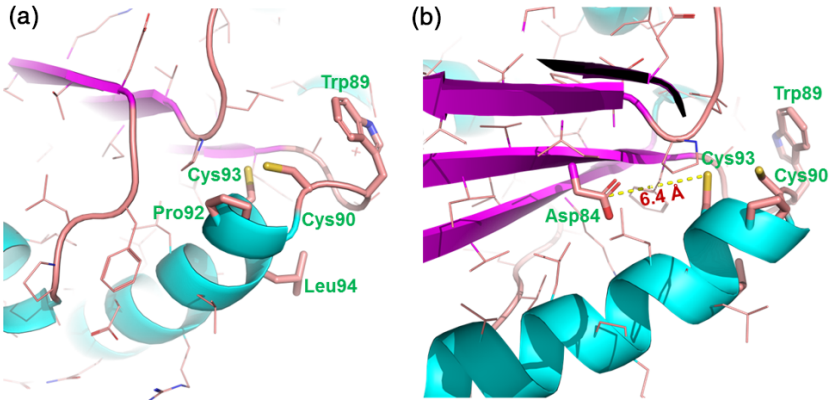

Figure 2. Redox site of CrTRXz. The main chain is represented as a cartoon. Side chains are represented as lines and colored according to atom type (blue = nitrogen, red = oxygen, yellow = sulfur).
(a) Redox site ^{89}WCPGCL^{94} side chains are highlighted in sticks and labeled as three-letter codes. C90 is located at the conserved nucleophile position.
(b) The nucleophile D84 side chain is shown as sticks. The carboxylate–thiol distance to C93 of 6.4 Å is drawn in a broken line.

asymmetric unit monomer and its closest neighbors. The available surface of a monomer is 6848 Å^2; hence, the largest 812.1-Å^2 interface covers 12% of the CrTRXz surface. This crystallographic A:B dimer is formed by subunit A at positions x, y, z and subunit B at positions $-x+2$, $-x+y+1$, $-z+2/3$ in a neighboring unit cell (Figure 3(a)). PISA computes a solvation free energy gain ($\Delta^i G$) of -11.3 kcal mol^{-1} upon formation of the interface. Twenty-one residues are located at the interface. Ten residues form hydrogen bonds between R77$_A$:E71$_B$, R149$_A$:M127$_B$, E71$_A$:R77$_B$, M127$_A$:R149$_B$, and at equivalent yet non-symmetrical positions R129$_A$:R129$_B$. Four residues form multiple salt bridges between R77$_A$:E71$_B$ and equivalent E71$_A$:R77$_B$. Overall, PISA scores this interface with a complexation significance of 1 (stable assembly), while the other five detected interfaces score at 0 (no stable assembly).

To try and probe the quaternary structure of CrTRXz in solution, we subjected two independent SEC-purified preparations of pure CrTRXz to small-angle X-ray scattering (SEC-SAXS) (Figure 3(b,c)). Guinier analysis radii of gyration of 20.16 ± 0.25 Å (protein preparation 1) and 23.34 ± 0.43 Å (preparation 2) allowed computation of respective molecular weight intervals of 15.80–17.75 kDa and 18.35–20.85 kDa at 95% credibility. The oligomeric state of CrTRXz detected by SAXS is consequently that of a monomer of 16.2 kDa. MS analysis of CrTRXz under native or denaturing conditions showed only the presence of monomeric species in our experimental conditions, suggesting that in solution CrTRXz is mainly monomeric.

In conclusion, the dimerization observed in crystal packing is too weak or too transitory to represent the principal protein population *in vitro* in the SAXS and MS experimental setups, while the higher apparent molecular weight on SEC may be due to non-globularity. The monomeric state is the most probable form expected in the diluted, non-crystalline physiological context.

CrTRXz reactive surface displays a unique electronegative potential

Multiplicity of TRX types in the chloroplast stroma raises the question of their specificity and the underlying physico-chemical determinants for selective and non-overlapping disulfide bond recognition in different targets (Lemaire *et al.*, 2007). In order to identify z-type specificities, we analyzed the high-resolution crystal structure of CrTRXz. The secondary structure topology is almost identical to those of other known TRXs (Figure S2). The redox residues are also positioned at the canonical sites and they form the most conserved surface of the protein among homologs (Figure 1(e,f)) (Ashkenazy *et al.*, 2016). The dynamics of the main chain are approximated by the crystallographic b-factors, the highest values of which are grouped at the N- and C-terminal ends and at the loop connecting strands 3 and 4 (Figure 1(g,h)). Helices 3 and 1 also group higher than average b-factors, albeit to a lower extent than the aforementioned loop and N/C-termini. This local flexibility may predict functional deformations of the CrTRXz structure upon folding, upon binding of protein partners, or during allosteric controls. All dynamic elements are however located far from the redox site and they are unlikely to contribute alone to the selectivity of CrTRXz towards targets.

The principal determinant of CrTRXf2 selectivity was described as an electropositive crown of residues exposed at the surface surrounding the redox site (Balmer *et al.*, 2004; Bunik *et al.*, 1999; Lemaire *et al.*, 2018; Yokochi *et al.*, 2019). We compared the electrostatic surface of CrTRXz and observed large electronegative patches and a general lack of electropositive elements (Figure 1(c,d)). Notably, CrTRXz presents the z-type conserved apolar L94 immediately after the redox site WCGPC, while all other plastidial TRX possess in this position either a positively charged

© 2021 Society for Experimental Biology and John Wiley & Sons Ltd,

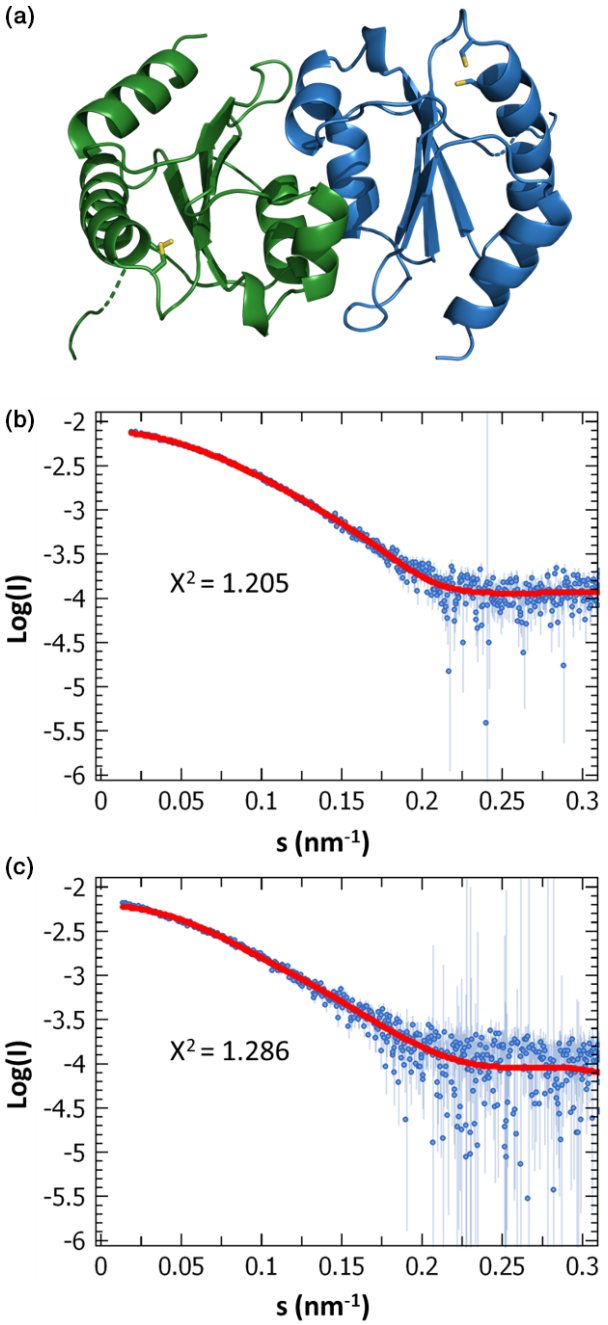

Figure 3. TRXz quaternary structure.
(a) Crystallographic dimer of CrTRXz represented in cartoon format with reactive cysteine side chains shown as sticks. Chain A is colored in blue, chain B in green.
(b) Small-angle X-ray scattering (SAXS) curve $\log(I) = f(s)$ of batch 1 of CrTRXz in blue was fitted to the crystallographic monomeric model of CrTRXz in red. (c) Same experiment as (b) with batch 2 of CrTRXz.

residue (R/K for m-, x-, and f-types) or a hydrogen bond donor residue (Q for y-type). Differential electrostatic repartition is particularly marked in the vicinity of the redox site and represents a significant qualitative difference with CrTRXf2 and CrTRXm equivalent surfaces (Figure 4(b,d,f)). The principal determinants of CrTRXf2 selectivity were proposed to be K78, K114, N130, K131, N133, K134, K143, and K164 (PDB ID: 6I1C) (Lemaire *et al.*, 2018). Equivalent positions on structurally aligned CrTRXz are occupied by E63, Q102, D119, E120, N121, P122, Q131, and E151. Seven out of these eight residues are conserved in TRXz homologs (Figure S1) and the electronegative surface is predicted to be conserved in a land plant ortholog (Figure S4), supporting an important function for type-z physiological functions in plants. In both CrTRXf2 and CrTRXz crystal structures, the aforementioned side chains are located at the protein surfaces and point their polar groups to the solvent. If the amino groups of lysines expose a +1 charge while the carboxyl groups of aspartates and glutamates expose a −1 charge at physiological pH, the aforementioned CrTRXf2 selectivity surface will accumulate a net charge of +6 while corresponding positions on CrTRXz sum a net charge of −4. The contributions of asparagine and glutamine residues to each selectivity surface are less explicit since they potentially behave as hydrogen bond donors or acceptors.

Overall, TRXz and TRXf2 recognition modes probably rely on distinct surface properties of targets because they present opposite electrostatic profiles. According to their mature sequence, CrTRXz presents an acidic isoelectric point while that of CrTRXf2 is basic (4.55 and 8.45, respectively). CrTRXm also presents an acidic isoelectric point (5.09), but important surface differences with CrTRXz stem from the charge repartition around the redox surface (Figures 4(b,d)).

TRXz is electro-complementary to known protein interactants

Four candidate proteins have been described as TRXz interactants in *A. thaliana*: FLN1, FLN2, PRIN2, and MRL7 (Arsova *et al.*, 2010; Diaz *et al.*, 2018; Yua *et al.*, 2014). The molecular structure of these proteins is not experimentally determined but their structures were predicted by homology using PHYRE software (Kelley *et al.*, 2015) (Figure 5). AtFLN1 possesses five cysteines and based on the protein model, adjacent C105 and C106 residues are buried within the structure and seem to be affected by TRX only in a solvent-exposed unfolded state. C204, C398, and C418 are predicted to be solvent-exposed and available for TRX redox interaction (Figure 5(a)) even though they probably do not form intramolecular disulfide bridges as they appear too distant. C398 is surrounded by an electropositive surface complementary to the CrTRXz recognition surface (Figure 5(b)). Homology-modeled AtFLN2 includes nine cysteines, where (i) the consecutive C208 and C209 are also located under the surface and probably not accessible in the folded state (Figure 5(c)), (ii) C290, C307, C322, C326, and C419 are present at the predicted surface, while (iii) C529 is hidden to solvent and C253 is at the bottom of

© 2021 Society for Experimental Biology and John Wiley & Sons Ltd,

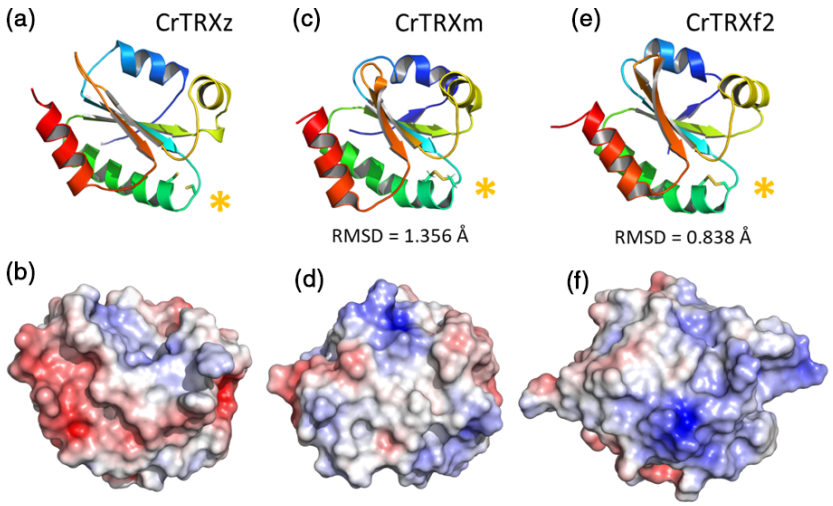

Figure 4. Structural comparison of plastidial TRX experimental structures. Root mean square deviations (RMSDs) between equivalent alpha carbons were calculated with PyMOL.
(a) CrTRXz crystal structure (this study) represented in cartoon format and colored from blue (N-terminus) to red (C-terminus). Cysteine side chains are shown as sticks and highlighted with an asterisk.
(b) Electrostatic surface potential of CrTRXz calculated with APBS (Baker *et al.*, 2001). Electronegative surface is colored in red while electropositive surface is colored in blue.
(c) CrTRXm nuclear magnetic resonance structure (Lancelin *et al.*, 2000) (PDB ID: 1DBY) represented and colored as in (a).
(d) Electrostatic surface potential of CrTRXm calculated with APBS and colored as in (b).
(e) CrTRXf2 crystal structure (PDB ID: 6I1C) represented and colored as in (a).
(f) Electrostatic surface potential calculated with APBS of CrTRXf2 and colored as in (b). APBS, Adaptive Poisson-Boltzman Solver.

a deep and narrow cleft. C290, C322, C326, and C327 are surrounded by electropositive surfaces that qualify them as potential targets of TRXz redox interaction (Figure 5(d)). The three latter would make good candidates for intramolecular dithiol/disulfide exchange since their thiols are predicted to be located at distances of 7.7, 8.5, and 9.2 Å. The AtMRL7 model encompasses two cysteines, both predicted at the solvent-exposed surface of the protein (Figure 5(e)). C281 is surrounded by marked electropositive potentials and may hence be targeted by the electrocomplementary TRXz redox surface (Figure 5(f)). AtPRIN2 could not be modeled by PHYRE as a globular structure, because of the lack of close homology with experimental models (best sequence identity 27% for 32% residue coverage, or 22% identity for 49% coverage). However, the 20-residue peptide NH_3^+-LSSLSRRGFVCRAAEYKFPDP-COO^- centered on redox target C68 (underlined) contains three arginines and one lysine and even though the mature protein sequence confers an acidic pI (4.43), the local environment of the cysteine in this peptide presents a basic pI of 9.31, which would make it a reasonable target for interaction with the TRXz electronegative surface.

CrTRXz can activate CrPRK *in vitro*

While CrPRK is a well-known CrTRXf2 target, presumably because of its partially negative surface around C55, another large positive patch is also present near C55 at the enzymatic pocket (Gurrieri *et al.*, 2019; Marri *et al.*, 2009). The mixed environment of CrPRK C55 suggests an independent, alternative mechanism of redox activation by TRXz. We probed the activation efficiency of CrTRXf2, CrTRXz, and CrTRXm on PRK activity. The ability of CrTRXs to reductively activate oxidized CrPRK was measured using different TRX:PRK ratios and assaying enzyme activity after 1 h of incubation (Figure 6). In every incubation, the concentration of CrPRK was 5 μM and the concentration of TRX varied from 0.5 μM (TRX:PRK ratio, 1:10) to 50 μM (TRX:PRK ratio, 10:1). At the lowest ratio (1:10), no TRX significantly activated PRK, while at higher ratios both CrTRXz and CrTRXf2 activated the enzyme. The CrTRXz activation plateaued at twofold excess, reaching 60% of maximal activity. No further activation was observed at higher TRX:PRK ratios. PRK activity in the presence of CrTRXf2 increased until sixfold excess, where 100% of maximal activity was obtained. CrTRXm was able to partially activate PRK only at the highest molar ratios (i.e., TRX:PRK ratios of 6:1 and 10:1). These results demonstrate that CrTRXf2 is the main activator for PRK *in vitro*, whereas CrTRXz is able to activate CrPRK to a lower extent.

DISCUSSION

Here, we report the experimental structure of TRXz from the model alga *C. reinhardtii* (PDB ID: 7ASW). Structural analysis reveals that chloroplastic CrTRXz is a classical

© 2021 Society for Experimental Biology and John Wiley & Sons Ltd,

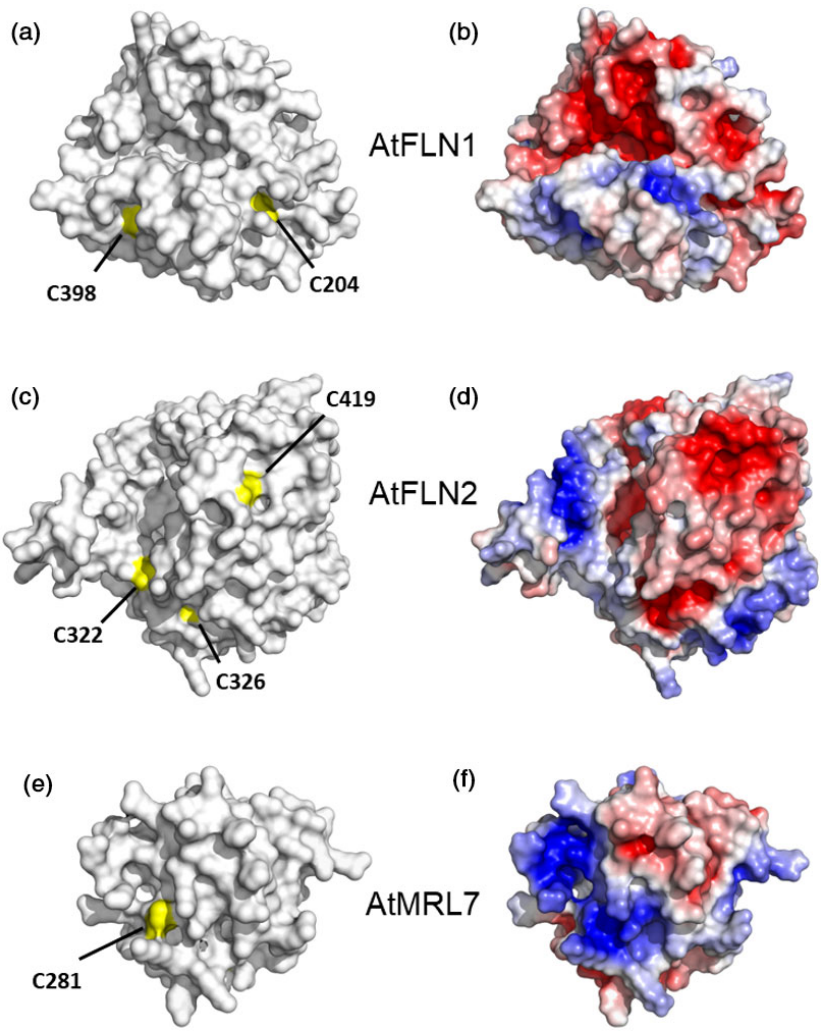

Figure 5. Electrostatic surface of PHYRE2 (Kelley *et al.*, 2015) homology-modeled TRXz protein partners.
(a) Connolly solvent exclusion surface of AtFLN1 residues 90–464 from the sequence of UniProt entry Q9M394 with cysteines in yellow.
(b) Electrostatic surface potential calculated with APBS. Electronegative surface is colored in red while electropositive surface is colored in blue (c). Connolly solvent exclusion surface of AtFLN2 205–557 from the sequence of UniProt entry F4I0K2 with cysteines in yellow.
(d) Electrostatic surface potential calculated with APBS and colored as in (b).
(e) Connolly solvent exclusion surface of AtMRL7 residues 195–312 from the sequence of UniProt entry F4JLC1 with cysteines in yellow.
(f) Electrostatic surface potential calculated with APBS and colored as in (a). APBS, Adaptive Poisson-Boltzman Solver.

TRX with an atypical electronegative surface conserved in plant homologs. We dissected TRXz surface properties to assess its putative specificity over known target proteins of AtTRXz. Moreover, based on structural features, we proposed the Calvin–Benson enzyme CrPRK as being recognized by CrTRXz, which was confirmed by our *in vitro* activity assays.

CrTRXz maintains the canonical fold of TRX

The determination of the crystal structure of chloroplastic TRXz from the green alga *C. reinhardtii* confirmed that it folds as a canonical αβα compact domain exposing the conserved WCGPC redox pentapeptide at nucleophile-attacking distance of incoming target disulfide bonds. Other signatures of reactivity and folding were observed in our structure, for example the base catalyst aspartate at a water-bridging distance to the resolving Cys_C, the 10-residue helix 1 of eukaryotic TRXs, and the folding bottleneck *cis*-P134. The reactive Cys redox pair appears dissociated in a dithiol state available for the reduction of a target disulfide bond.

CrTRXz evolved distinct features

Although conforming to the TRX standard, our crystal structure reveals distinct features of CrTRXz. The peptide connecting strand 2 and helix 3 is folded as a short helix

© 2021 Society for Experimental Biology and John Wiley & Sons Ltd,

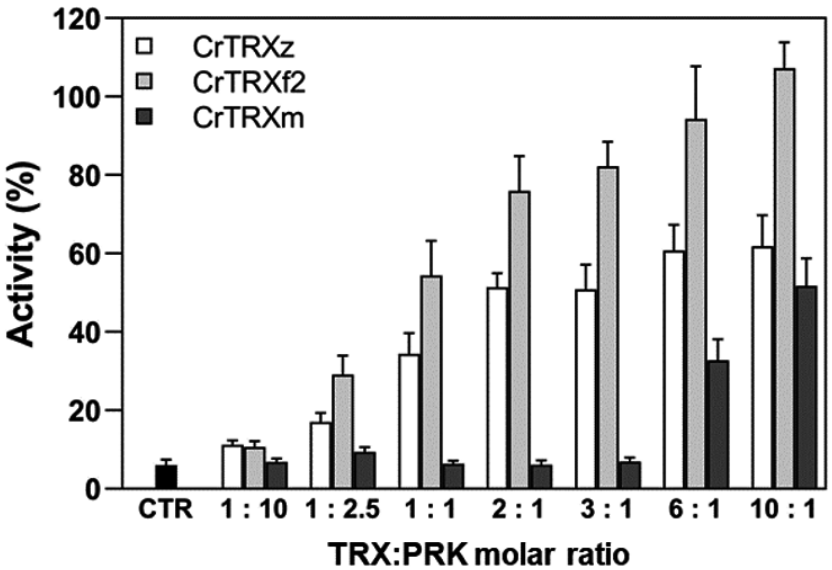

Figure 6. Activation efficiency of CrTRXz, CrTRXf2, and CrTRXm on CrPRK. Activation of oxidized CrPRK (5 μM) after 1 h incubation with increasing concentrations (0.5–50 μM) of CrTRXz (white bars), CrTRXf2 (light gray bars), and CrTRXm (dark gray bars) in the presence of 0.2 mM DTT. TRX:PRK ratios are indicated for each tested condition. Control sample (CTR, black bar) shows the activity after incubation with 0.2 mM DTT without TRXs. All activities were normalized to fully activated PRK obtained after 4 h of reduction with 40 mM DTT. Data are reported as mean ± standard deviation (n = 3). DTT, dithiothreitol; PRK, phosphoribulokinase.

3_{10} that is stabilized by hydrogen-bonding interaction of D119 with W89, adjacent to Cys_N in the redox site. This particular state may modify the reactivity of the TRXz active site or rather a functional conformation of TRX since D119 is conserved in CrTRXx, y, h1, h2, and o while it is substituted by an isosteric asparagine in CrTRXf2 and m. C126 of AtTRXf1 was shown to be glutathionylated and the glutathionylation demonstrated to subsequently affect the redox capacity of this TRX (Michelet *et al.*, 2005). CrTRXf1 and f2 but not the other TRX types possess this regulatory cysteine, at the first position after the aforementioned D119 or its equivalents. Hence, regulation of TRX by redox signaling may be caused by distal effects on the redox site through a bonding network similar to CrTRXz D119–W89. Interestingly, selective inactivation of TRXf by glutathionylation would leave TRXz as an alternative to perform photosynthetic functions such as light- and TRX-dependent activations of PRK.

CrTRXz crystallizes as a homodimer and elutes as larger than globular monomer objects as judged by SEC. SAXS and native mass spectrometry however unequivocally contradicted the dimer hypothesis in solution, with the measured gyration radii and diffusion curves revealing a monomeric state of globular CrTRXz *in vitro*. Dimerization is either a pure crystallization artifact or a transitory interaction in restricted conditions of high local concentration, like those of a liquid–liquid phase separation or of a multiprotein complex. The interaction surface is distant from the redox site and may rather serve to scaffold TRXz-containing complexes with internal twofold symmetries. Other TRX quaternary states were tested in the past and TRX proved monomeric (Capitani and Schurmann, 2004; Gronenborn *et al.*, 1999) in the reduced state (Weichsel *et al.*, 1996).

Electronegativity as a driver of CrTRXz-specific complexation

Western blot protein quantification of *A. thaliana* leaf extracts indicated relative abundances of 69.1% TRXm, 22.2% TRXf, 6.3% TRXx, 1.3% TRXy, and 1.1% TRXz, representing a TRXz concentration of 1–5 pmol mg^{-1} stromal protein (Okegawa and Motohashi, 2015). Notwithstanding its relative scarcity, TRXz still makes significant contributions to chloroplast functions, as demonstrated by the lethality of its deletion mutant. We propose that TRXz loss cannot be compensated by other TRXs because of the irreplaceable specialization of its electronegative surface. Described determinants of TRXf2 selectivity present an opposite, electropositive character compared to TRXz. Reported targets of TRXz in *A. thaliana* present exposed cysteines on electropositive surfaces that match the TRXz redox site (Figure 5). One interesting candidate for interaction is TRXf itself, since the electropositive environment of its active site is an ideal electro-complementary platform for TRXz docking. Consistently, TRXz was reported to be reduced *in vitro* by FTR (Chibani *et al.*, 2011) but also by other TRX types (Bohrer *et al.*, 2012), suggesting that it could play a specific role in reductive or oxidant signaling (Bohrer *et al.*, 2012; Yoshida and Hisabori, 2016).

© 2021 Society for Experimental Biology and John Wiley & Sons Ltd,

We report here that CrTRXz is able to activate CrPRK, a known target of the main CBC activator TRXf2. CrTRXz activation is slightly weaker than that of CrTRXf2 but stronger than CrTRXm activation. It relies on the ratio between TRX and target, so TRXz could efficiently activate PRK or other targets when it reaches a certain concentration in the chloroplast. Interestingly, the cell has at its disposal two different TRXs to activate PRK and tune the CBC flux according to environmental conditions. In conditions when TRXf2 is inactivated by glutathionylation (Michelet *et al.*, 2005), one can hypothesize that TRXz becomes the replacement activator of PRK.

TRX complementarities should now be confirmed by the description of the actual complexes between TRX and targets, ideally from experimental structures at atomic resolution. TRXm, x, and y in the chloroplast still await a comprehensive description of the molecular basis for specific disulfide targeting, as well as TRXh/TRXo and bacterial TRX in their respective compartments. Later on, a global simulation of electron transfers in the proteome will require knowledge on the concentrations of all TRXs, reductant sources, and targets, their mutual binding affinities, interaction turnovers, and their cysteine redox potentials.

EXPERIMENTAL PROCEDURES

Cloning

The amino acid sequence of the nuclear-encoded *C. reinhardtii* TRXz (UniRef100 entry A8J0Q8, TRX-related protein CITRX) was analyzed by TargetP2.0 (Almagro Armenteros *et al.*, 2019; Emanuelsson *et al.*, 2007), ChloroP (Emanuelsson *et al.*, 1999), and Predalgo (Tardif *et al.*, 2012) to predict the transit peptide cutting site and the subsequent mature sequence of chloroplastic protein. The sequence coding for amino acids 56–183 was PCR-amplified from *C. reinhardtii* expressed sequence tags database plasmid AV642845 with DNA primers 5′-TGTCGC**CATATG**GTCATTAGCCATGGAAAG-3′ and 5′-CTCCTT**AAGCTT**CTACTGCTGCGGCGCCTCGGG-3′. The PCR product was inserted into pET28a by restriction with *Nde*I and *Hin*dIII and subsequent ligation, yielding pET28a-His_6-CrTRXz. Recombinant protein is a fusion of Met-HHHHHH-SSFLVPRGSHM- and TRXz residues 56–183, as validated by plasmid Sanger sequencing. Residue numbering is in accordance with UniProt sequence A8J0Q8-1 throughout the text.

Expression and purification

Escherichia coli strain BL21(DE3) Rosetta-2 pLysS (Novagen Merck, Darmstadt, Germany) was transformed with pET28a-His6-CrTRXz and grown in 1 L of 2YT medium supplemented with kanamycin (50 μg ml^{-1}) and chloramphenicol (34 μg ml^{-1}) to the exponential phase at an optical density of 0.6 before induction of overexpression with 200 μM isopropyl β-D-1-thiogalactopyranoside for 3.5 h at 37°C. Cell pellet (4.1 g) was resuspended in 20 ml buffer A (20 mM Tris-Cl pH 7.9, 200 mM NaCl) and lysed by 2 min sonication with 0.4-sec pulses at output 5 on a W-375 sonicator equipped with a microtip (Qsonica, Newtown, CT, USA) on ice. Total extract was clarified by 20 min centrifugation at 30 000 *g* at 4°C and the soluble fraction was loaded on an affinity chromatograph over 5 ml of NiNTA resin (Sigma-Aldrich Merck, Darmstadt, Germany). Resin was step-washed with 10 ml of buffer A supplemented with 10, 20, 30, 40, or 50 mM imidazole. Elution was executed with steps of 10 ml of buffer A supplemented with 100, 150, 200, or 250 mM imidazole. Collected fractions were analyzed by SDS-PAGE and Coomassie staining, revealing the presence of >99% pure TRXz in wash fractions 20, 30, 40, and 50 and elution fractions 100 and 200. Pooled fractions were buffer-exchanged to buffer A and concentrated by ultrafiltration on 3000 MWCO Amicon filter units (Millipore Merck, Darmstadt, Germany). A final concentration of 10.2 mg ml^{-1} was measured by a NanoDrop 2000 spectrophotometer (Thermo Fisher Scientific, Waltham, MA, USA) with theoretical Mw = 16 191.5 g mol^{-1} and ε_{280} = 5567.5 mol^{-1} L cm^{-1}.

Size-exclusion chromatography

Affinity-purified recombinant CrTRXz (0.1 mg) was loaded on a Superose6 10/300 Increase column or a BioSEC3-300 column in 20 mM Tris-Cl pH 7.9, 100 mM NaCl. Isocratic elution was recorded at 280 nm.

Small-angle X-ray scattering. Diffusion curves were collected from a BioSEC3-300 SEC in line with an X-ray exposure capillary at the beamline SWING of Synchrotron SOLEIL (Saint-Aubin, France). Data were processed with FOXTROT (Xenocs, Grenoble France) using CLEVERAVG algorithms and interpreted with ATSAS (Petoukhov *et al.*, 2012; Franke *et al.*, 2017).

Crystallization and structure determination

Purified CrTRXz was tested for crystallization in commercial sparse-screening conditions (Qiagen, Hilden, Germany) of the Joint Center for Structural Genomics screens (Lesley and Wilson, 2005) with a mixture of 30 nl protein and 30 nl precipitant equilibrated against a reservoir volume of 30 μl mother liquor. Monocrystals sized 30 μm grew in 1 week in condition 38 at position D2 of screen IV (0.1 M HEPES pH 7.5, 1.26 M ammonium sulfate). Crystals were transferred in mother liquor supplemented with 12.5% glycerol and flash-frozen in liquid nitrogen for diffraction experiments at a micro-focused beamline PROXIMA-2A at a SOLEIL synchrotron (Saint-Aubin, France). A 99.36% complete dataset was collected at 2.444 Å resolution. Data were indexed in space group $P3_221$, integrated, scaled, and converted with XDSME (Legrand, 2017). The structure was phased by molecular replacement with PHENIX (Adams *et al.*, 2010, 2011) and PHASER-MR (McCoy *et al.*, 2007) using CrTRXf2 (PDB ID: 6I1C) (Lemaire *et al.*, 2018) as a search model and a single protein in the asymmetric unit. The model was refined by iterative cycles of manual building in COOT (Emsley and Cowtan, 2004; Emsley *et al.*, 2010) followed by refinement with PHENIX.REFINE (Afonine *et al.*, 2012) until completion of a structure passing MOLPROBITY (Chen *et al.*, 2010) evaluation with 100% residues for Ramachandran restrains RMS (bonds) = 0.010, RMS (angles) = 1.44 and final R_{work} = 0.2296, R_{free} = 0.2335 (Table 1). Structure representations were drawn with PyMOL (Schrodinger, New York, NY, USA).

TRX activation assay

CrPRK was recombinantly expressed as published earlier (Gurrieri *et al.*, 2019). Pure CrPRK was oxidized in the presence of 0.2 mM 5,5′-dithiobis(2-nitrobenzoic acid) (Sigma-Aldrich, Darmstadt, Germany) for 45 min at room temperature. CrPRK was desalted to stop the oxidation and used to assay TRX activation efficiency. Oxidized CrPRK at 5 μM was incubated in the presence of 0.2 mM dithiothreitol (DTT) and 0.5–50 μM CrTRXz, CrTRXf2, and CrTRXm

© 2021 Society for Experimental Biology and John Wiley & Sons Ltd,

for 60 min. PRK activity was assayed as in Gurrieri *et al.* (2019). Control activity was obtained incubating CrPRK with 0.2 mM DTT for 60 min. Activities were normalized on fully reduced PRK obtained after 4 h incubation at room temperature in the presence of 40 mM DTT.

ACKNOWLEDGMENTS

This work was funded by CNRS, Sorbonne Université, and Agence Nationale de la Recherche grants LABEX DYNAMO 11-LABX-0011, CALVINDESIGN (ANR-17-CE05-001), and CALVINTERACT (ANR-19-CE11-0009). Libero Gurrieri was supported by grant PON ARS01 00881 'ORIGAMI' (Italian Ministry of University and Research). Fernanda Pires Borrega and Sandrine Hoang contributed to the preparation of recombinant thioredoxin z. The Institut de Biologie Physico-Chimique (FR 550 CNRS) provided access to crystallization facilities. We acknowledge SOLEIL for provision of synchrotron radiation facilities. We thank Martin Savko, Serena Sirigu, and William Shepard for assistance in using the beamline PROXIMA-2a and Aurélien Thureau and Javier Perez for assistance in using the beamline SWING.

AUTHOR CONTRIBUTIONS

Conception, MZ, FS, SDL, and JH; acquisition and analysis of data, TLM, LG, CHM, and JH; manuscript writing, reviewing, and editing, TLM, LG, PC, CHM, MZ, FS, SDL, and JH; funding and resource acquisition, FS, SDL, and JH. All authors have read and agreed to the final version of the manuscript.

CONFLICT OF INTEREST

The authors have no conflicts of interest to declare.

DATA AVAILABILITY STATEMENT

Validated crystallographic reflection data and the model are deposited in the Protein Data Bank under identifier 7ASW.

SUPPORTING INFORMATION

Additional Supporting Information may be found in the online version of this article.

Figure S1. Sequence alignment of CrTRXz homologs. Sequence alignment was performed by Clustal Omega with homologs from different species. Residues with more than 50% conservation are colored in red, and strictly conserved residues are shown in white with a red background. Numbering is in accordance with the sequence of thioredoxin z (TRXz) from *Chlamydomonas reinhardtii*. TRX sequences were retrieved from the UniProtKB database for the following species: *C. reinhardtii* (A8J0Q8), *Gonium pectorale* (A0A150FZQ6), *Tetrabaena socialis* (A0A2J7ZQ73), *Volvox carteri* f. *nagariensis* (D8TVT1), *Ostreococcus tauri* (A0A1Y5IIS5), *Arabidopsis thaliana* (Q9M7X9), *Synechocystis* sp. *PCC 6714* (A0A068MSG5), and *Glycine max* (I1JW39).

Figure S2. CrTRX experimental structures. (a) Side and top views of the CrTRXz structure. CrTRXz is represented in cartoon format and colored in rainbow colors from the N-terminus (blue) to the C-terminus (red). Reactive cysteine side chains are represented in sticks. (b) CrTRXm in the same orientation, representation, and coloration as in (a). (c) CrTRXf2 in the same orientation, representation, and coloration as in (a). (d) Structural alignment of CrTRXf2, CrTRXm, and CrTRXh structures colored in white on the CrTRXz structure colored in green, realized by PyMOL. Root mean square deviation (RMSD) values of alignments are 1.357, 0.838, and 1.123 Å for CrTRXm, CrTRXf2, and CrTRXh, respectively.

Figure S3. CrTRXz size-exclusion chromatography. High-pressure liquid chromatography profile over a BioSEC3-300 column of (a) preparation 1 and (b) preparation 2 of CrTRXz. Globular calibration standards are eluted at 7.2 ml (670 kDa), 9.2 ml (158 kDa), 10.6 ml (44 kDa), and 11.7 ml (17 kDa). Dead column volume is 6.5 ml and total column volume is 13.4 ml. TRXz peaks are indicated by green arrows.

Figure S4. Comparison of homology models of *A. thaliana* TRXz computed from the sequence in UniProt entry Q9M7X9 isoform 1 with the experimental structure of *C. reinhardtii* TRXz. Structures align with RMSD values of 1.1–1.4 Å. Nucleophilic cysteine side chains are displayed as spheres with sulfur in gold. (a) *Arabidopsis thaliana* TRXz SWISS-MODEL analysis by homology with 50 template thioredoxins. (b) Experimental crystal structure of *C. reinhardtii* TRXz (this study). (c) Comparison of an *A. thaliana* TRXz model to an ortholog with 24% sequence identity using Phyre2 with a confidence score of 99/100. (d) Electrostatic potential of AtTRXz, as determined using SWISS-MODEL. (e) Electrostatic potential of the CrTRXz crystal structure. (f) Electrostatic potential of the AtTRXz Phyre2 model. Potential is colored from red (negative) to blue (positive).

REFERENCES

Adams, P.D., Afonine, P.V., Bunkoczi, G., Chen, V.B., Davis, I.W., Echols, N. *et al.* (2010) PHENIX: A comprehensive Python-based system for macromolecular structure solution. *Acta Crystallographica Section D: Biological Crystallography*, **66**, 213–221.

Adams, P.D., Afonine, P.V., Bunkoczi, G., Chen, V.B., Echols, N., Headd, J.J. *et al.* (2011) The Phenix software for automated determination of macromolecular structures. *Methods*, **55**, 94–106.

Afonine, P.V., Grosse-Kunstleve, R.W., Echols, N., Headd, J.J., Moriarty, N.W., Mustyakimov, M. *et al.* (2012) Towards automated crystallographic structure refinement with phenix.refine. *Acta Crystallographica Section D: Biological Crystallography*, **68**, 352–367.

Almagro Armenteros, J.J., Salvatore, M., Emanuelsson, O., Winther, O., Von Heijne, G., Elofsson, A. *et al.* (2019) Detecting sequence signals in targeting peptides using deep learning. *Life Science Alliance*, **2**.

Arsova, B., Hoja, U., Wimmelbacher, M., Greiner, E., Ustun, S., Melzer, M. *et al.* (2010) Plastidial thioredoxin z interacts with two fructokinase-like proteins in a thiol-dependent manner: Evidence for an essential role in chloroplast development in *Arabidopsis* and *Nicotiana benthamiana*. *The Plant Cell*, **22**, 1498–1515.

Ashkenazy, H., Abadi, S., Martz, E., Chay, O., Mayrose, I., Pupko, T. *et al.* (2016) ConSurf 2016: An improved methodology to estimate and visualize evolutionary conservation in macromolecules. *Nucleic Acids Research*, **44**, W344–W350.

Avilan, L., Puppo, C., Erales, J., Woudstra, M., Lebrun, R. & Gontero, B. (2012) CP12 residues involved in the formation and regulation of the glyceraldehyde-3-phosphate dehydrogenase-CP12-phosphoribulokinase complex in *Chlamydomonas reinhardtii*. *Molecular Biosystems*, **8**, 2994–3002.

Baker, N.A., Sept, D., Joseph, S., Holst, M.J. & Mccammon, J.A. (2001) Electrostatics of nanosystems: Application to microtubules and the ribosome. *Proceedings of the National Academy of Sciences of the United States of America*, **98**, 10037–10041.

Balmer, Y., Koller, A., Val, G.D., Schurmann, P. & Buchanan, B.B. (2004) Proteomics uncovers proteins interacting electrostatically with thioredoxin in chloroplasts. *Photosynthetic Research*, **79**, 275–280.

Balsera, M., Uberegui, E., Schurmann, P. & Buchanan, B.B. (2014) Evolutionary development of redox regulation in chloroplasts. *Antioxidants and Redox Signaling*, **21**, 1327–1355.

Bedhomme, M., Adamo, M., Marchand, C.H., Couturier, J., Rouhier, N., Lemaire, S.D. *et al.* (2012) Glutathionylation of cytosolic glyceraldehyde-3-phosphate dehydrogenase from the model plant *Arabidopsis thaliana*

© 2021 Society for Experimental Biology and John Wiley & Sons Ltd,

is reversed by both glutaredoxins and thioredoxins in vitro. *Biochemical Journal*, **445**, 337–347.

Benhar, M., Forrester, M.T., Hess, D.T. & Stamler, J.S. (2008) Regulated protein denitrosylation by cytosolic and mitochondrial thioredoxins. *Science*, **320**, 1050–1054.

Berger, H., De Mia, M., Morisse, S., Marchand, C.H., Lemaire, S.D., Wobbe, L. *et al.* (2016) A light switch based on protein S-nitrosylation fine-tunes photosynthetic light harvesting in *Chlamydomonas*. *Plant Physiology*, **171**, 821–832.

Blomback, B., Blomback, M., Finkbeiner, W., Holmgren, A., Kowalska-Loth, B. & Olovson, G. (1974) Enzymatic reduction of disulfide bonds in fibrinogen by the thioredoxin system. I. Identification of reduced bonds and studies on reoxidation process. *Thrombosis Research*, **4**, 55–75.

Bohrer, A.S., Massot, V., Innocenti, G., Reichheld, J.P., Issakidis-Bourguet, E. & Vanacker, H. (2012) New insights into the reduction systems of plastidial thioredoxins point out the unique properties of thioredoxin z from *Arabidopsis*. *Journal of Experimental Botany*, **63**, 6315–6323.

Buchanan, B.B., Holmgren, A., Jacquot, J.P. & Scheibe, R. (2012) Fifty years in the thioredoxin field and a bountiful harvest. *Biochimica et Biophysica Acta*, **1820**, 1822–1829.

Bunik, V., Raddatz, G., Lemaire, S., Meyer, Y., Jacquot, J.P. & Bisswanger, H. (1999) Interaction of thioredoxins with target proteins: Role of particular structural elements and electrostatic properties of thioredoxins in their interplay with 2-oxoacid dehydrogenase complexes. *Protein Science*, **8**, 65–74.

Capitani, G. & Schurmann, P. (2004) On the quaternary assembly of spinach chloroplast thioredoxin m. *Photosynthetic Research*, **79**, 281–285.

Cejudo, F.J., Ojeda, V., Delgado-Requerey, V., Gonzalez, M. & Perez-Ruiz, J.M. (2019) Chloroplast redox regulatory mechanisms in plant adaptation to light and darkness. *Frontiers in Plant Science*, **10**, 380.

Chen, V.B., Arendall, W.B. 3rd, Headd, J.J., Keedy, D.A., Immormino, R.M., Kapral, G.J. *et al.* (2010) MolProbity: All-atom structure validation for macromolecular crystallography. *Acta Crystallographica Section D: Biological Crystallography*, **66**, 12–21.

Chibani, K., Tarrago, L., Schürmann, P., Jacquot, J.P. & Rouhier, N. (2011) Biochemical properties of poplar thioredoxin z. *FEBS Letters*, **585**.

Chivers, P.T. & Raines, R.T. (1997) General acid/base catalysis in the active site of *Escherichia coli* thioredoxin. *Biochemistry*, **36**, 15810–15816.

Collin, V., Issakidis-Bourguet, E., Marchand, C., Hirasawa, M., Lancelin, J.M., Knaff, D.B. *et al.* (2003) The *Arabidopsis* plastidial thioredoxins: New functions and new insights into specificity. *Journal of Biological Chemistry*, **278**, 23747–23752.

De Lamotte-Guery, F., Miginiac-Maslow, M., Decottignies, P., Stein, M., Minard, P. & Jacquot, J.P. (1991) Mutation of a negatively charged amino acid in thioredoxin modifies its reactivity with chloroplastic enzymes. *European Journal of Biochemistry*, **196**, 287–294.

Diaz, M.G., Hernandez-Verdeja, T., Kremnev, D., Crawford, T., Dubreuil, C. & Strand, A. (2018) Redox regulation of PEP activity during seedling establishment in *Arabidopsis thaliana*. *Nature Communications*, **9**, 50.

Emanuelsson, O., Brunak, S., Von Heijne, G. & Nielsen, H. (2007) Locating proteins in the cell using TargetP, SignalP and related tools. *Nature Protocols*, **2**, 953–971.

Emanuelsson, O., Nielsen, H. & Von Heijne, G. (1999) ChloroP, a neural network-based method for predicting chloroplast transit peptides and their cleavage sites. *Protein Science*, **8**, 978–984.

Emsley, P. & Cowtan, K. (2004) Coot: Model-building tools for molecular graphics. *Acta Crystallographica Section D: Biological Crystallography*, **60**, 2126–2132.

Emsley, P., Lohkamp, B., Scott, W.G. & Cowtan, K. (2010) Features and development of Coot. *Acta Crystallographica Section D: Biological Crystallography*, **66**, 486–501.

Ferrer-Sueta, G., Manta, B., Botti, H., Radi, R., Trujillo, M. & Denicola, A. (2011) Factors affecting protein thiol reactivity and specificity in peroxide reduction. *Chemical Research in Toxicology*, **24**, 434–450.

Franke, D., Petoukhov, M.V., Konarev, P.V., Panjkovich, A., Tuukkanen, A., Mertens, H.D.T. *et al.* (2017) ATSAS 2.8: A comprehensive data analysis suite for small-angle scattering from macromolecular solutions. *Journal of Applied Crystallography*, **50**, 1212–1225.

Gamiz-Arco, G., Risso, V.A., Candel, A.M., Ingles-Prieto, A., Romero-Romero, M.L., Gaucher, E.A. *et al.* (2019) Non-conservation of folding rates in the thioredoxin family reveals degradation of ancestral unassisted-folding. *Biochemical Journal*.

Gleason, F.K. & Holmgren, A. (1981) Isolation and characterization of thioredoxin from the cyanobacterium, *Anabaena* sp. *Journal of Biological Chemistry*, **256**, 8306–8309.

Gonzalez Porque, P., Baldesten, A. & Reichard, P. (1970) Purification of a thioredoxin system from yeast. *Journal of Biological Chemistry*, **245**, 2363–2370.

Greetham, D., Vickerstaff, J., Shenton, D., Perrone, G.G., Dawes, I.W. & Grant, C.M. (2010) Thioredoxins function as deglutathionylase enzymes in the yeast *Saccharomyces cerevisiae*. *BMC Biochemistry*, **11**, 3.

Gronenborn, A.M., Clore, G.M., Louis, J.M. & Wingfield, P.T. (1999) Is human thioredoxin monomeric or dimeric? *Protein Science*, **8**, 426–429.

Gurrieri, L., Del Giudice, A., Demitri, N., Falini, G., Pavel, N.V., Zaffagnini, M. *et al.* (2019) *Arabidopsis* and *Chlamydomonas* phosphoribulokinase crystal structures complete the redox structural proteome of the Calvin-Benson cycle. *Proceedings of the National Academy of Sciences of the United States of America*, **116**, 8048–8053.

Gutle, D.D., Roret, T., Muller, S.J., Couturier, J., Lemaire, S.D., Hecker, A. *et al.* (2016) Chloroplast FBPase and SBPase are thioredoxin-linked enzymes with similar architecture but different evolutionary histories. *Proceedings of the National Academy of Sciences of the United States of America*, **113**, 6779–6784.

Hall, D.E., Baldesten, A., Holmgren, A. & Reichard, P. (1971) Yeast thioredoxin. Amino-acid sequence around the active-center disulfide of thioredoxin I and II. *European Journal of Biochemistry*, **23**, 328–335.

Hanschmann, E.M., Godoy, J.R., Berndt, C., Hudemann, C. & Lillig, C.H. (2013) Thioredoxins, glutaredoxins, and peroxiredoxins-molecular mechanisms and health significance: From cofactors to antioxidants to redox signaling. *Antioxidants and Redox Signaling*, **19**, 1539–1605.

Hirasawa, M., Schurmann, P., Jacquot, J.P., Manieri, W., Jacquot, P., Keryer, E. *et al.* (1999) Oxidation-reduction properties of chloroplast thioredoxins, ferredoxin:thioredoxin reductase, and thioredoxin f-regulated enzymes. *Biochemistry*, **38**, 5200–5205.

Holmgren, A. (1968) Thioredoxin. 6. The amino acid sequence of the protein from *Escherichia coli* B. *European Journal of Biochemistry*, **6**, 475–484.

Holmgren, A., Buchanan, B.B. & Wolosiuk, R.A. (1977) Photosynthetic regulatory protein from rabbit liver is identical with thioredoxin. *FEBS Letters*, **82**, 351–354.

Holmgren, A. & Morgan, F.J. (1976) Enzyme reduction of disulfide bonds by thioredoxin. The reactivity of disulfide bonds in human choriogonadotropin and its subunits. *European Journal of Biochemistry*, **70**, 377–383.

Huang, C., Yu, Q.B., Lv, R.H., Yin, Q.Q., Chen, G.Y., Xu, L. *et al.* (2013) The reduced plastid-encoded polymerase-dependent plastid gene expression leads to the delayed greening of the *Arabidopsis* fln2 mutant. *PLoS One*, **8**, e73092.

Huppe, H.C. & Buchanan, B.B. (1989) Activation of a chloroplast type of fructose bisphosphatase from *Chlamydomonas reinhardtii* by light-mediated agents. *Zeitschrift für Naturforschung C: A Journal of Biosciences*, **44**, 487–494.

Ingles-Prieto, A., Ibarra-Molero, B., Delgado-Delgado, A., Perez-Jimenez, R., Fernandez, J.M., Gaucher, E.A. *et al.* (2013) Conservation of protein structure over four billion years. *Structure*, **21**, 1690–1697.

Jacquot, J.P., Eklund, H., Rouhier, N. & Schurmann, P. (2009) Structural and evolutionary aspects of thioredoxin reductases in photosynthetic organisms. *Trends in Plant Science*, **14**, 336–343.

Kang, Z., Qin, T. & Zhao, Z. (2019) Thioredoxins and thioredoxin reductase in chloroplasts: A review. *Gene*, **706**, 32–42.

Kelley, L.A. Mezulis, S., Yates, C.M., Wass, M.N. & Sternberg, M.J.(2015) The Phyre2 web portal for protein modeling, prediction and analysis. *Nature Protocols*, **10**, 845–858.

Kelley, R.F. & Richards, F.M. (1987) Replacement of proline-76 with alanine eliminates the slowest kinetic phase in thioredoxin folding. *Biochemistry*, **26**, 6765–6774.

Konig, J., Muthuramalingam, M. & Dietz, K.J. (2012) Mechanisms and dynamics in the thiol/disulfide redox regulatory network: Transmitters, sensors and targets. *Current Opinions in Plant Biology*, **15**, 261–268.

Kulczyk, A.W., Moeller, A., Meyer, P., Sliz, P. & Richardson, C.C. (2017) Cryo-EM structure of the replisome reveals multiple interactions

© 2021 Society for Experimental Biology and John Wiley & Sons Ltd,

coordinating DNA synthesis. *Proceedings of the National Academy of Sciences of the United States of America*, **114**, E1848–E1856.

Lancelin, J.M., Guilhaudis, L., Krimm, I., Blackledge, M.J., Marion, D. & Jacquot, J.P. (2000) NMR structures of thioredoxin m from the green alga *Chlamydomonas reinhardtii*. *Proteins*, **41**, 334–349.

Lee, S., Kim, S.M. & Lee, R.T. (2013) Thioredoxin and thioredoxin target proteins: From molecular mechanisms to functional significance. *Antioxidants and Redox Signaling*, **18**, 1165–1207.

Legrand, P. (2017) XDSME: XDS Made Easier.

Lemaire, S.D., Guillon, B., Le Marechal, P., Keryer, E., Miginiac-Maslow, M. & Decottignies, P. (2004) New thioredoxin targets in the unicellular photosynthetic eukaryote *Chlamydomonas reinhardtii*. *Proceedings of the National Academy of Sciences of the United States of America*, **101**, 7475–7480.

Lemaire, S.D., Michelet, L., Zaffagnini, M., Massot, V. & Issakidis-Bourguet, E. (2007) Thioredoxins in chloroplasts. *Current Genetics*, **51**, 343–365.

Lemaire, S.D., Tedesco, D., Crozet, P., Michelet, L., Fermani, S., Zaffagnini, M. *et al.* (2018) Crystal structure of chloroplastic thioredoxin f2 from *Chlamydomonas reinhardtii* reveals distinct surface properties. *Antioxidants (Basel)*, **7**.

Lemaster, D.M., Springer, P.A. & Unkefer, C.J. (1997) The role of the buried aspartate of *Escherichia coli* thioredoxin in the activation of the mixed disulfide intermediate. *Journal of Biological Chemistry*, **272**, 29998–30001.

Lesley, S.A. & Wilson, I.A. (2005) Protein production and crystallization at the joint center for structural genomics. *Journal of Structural and Functional Genomics*, **6**, 71–79.

Liebthal, M., Maynard, D. & Dietz, K.J. (2018) Peroxiredoxins and redox signaling in plants. *Antioxidants and Redox Signaling*, **28**, 609–624.

Lillig, C.H. & Holmgren, A. (2007) Thioredoxin and related molecules—from biology to health and disease. *Antioxidants and Redox Signaling*, **9**, 25–47.

Marchand, C.H., Fermani, S., Rossi, J., Gurrieri, L., Tedesco, D., Henri, J. *et al.* (2019) Structural and biochemical insights into the reactivity of thioredoxin h1 from *Chlamydomonas reinhardtii*. *Antioxidants (Basel)*, **8**.

Marri, L., Zaffagnini, M., Collin, V., Issakidis-Bourguet, E., Lemaire, S.D., Pupillo, P. *et al.* (2009) Prompt and easy activation by specific thioredoxins of calvin cycle enzymes of *Arabidopsis thaliana* associated in the GAPDH/CP12/PRK supramolecular complex. *Molecular Plant*, **2**, 259–269.

Mccoy, A.J., Grosse-Kunstleve, R.W., Adams, P.D., Winn, M.D., Storoni, L.C. & Read, R.J. (2007) Phaser crystallographic software. *Journal of Applied Crystallography*, **40**, 658–674.

Menchise, V., Corbier, C., Didierjean, C., Saviano, M., Benedetti, E., Jacquot, J.P. *et al.* (2001) Crystal structure of the wild-type and D30A mutant thioredoxin h of *Chlamydomonas reinhardtii* and implications for the catalytic mechanism. *Biochemical Journal*, **359**, 65–75.

Michelet, L., Zaffagnini, M., Marchand, C., Collin, V., Decottignies, P., Tsan, P. *et al.* (2005) Glutathionylation of chloroplast thioredoxin f is a redox signaling mechanism in plants. *Proceedings of the National Academy of Sciences of the United States of America*, **102**, 16478–16483.

Michelet, L., Zaffagnini, M., Massot, V., Keryer, E., Vanacker, H., Miginiac-Maslow, M. *et al.* (2006) Thioredoxins, glutaredoxins, and glutathionylation: New crosstalks to explore. *Photosynthetic Research*, **89**, 225–245.

Michelet, L., Zaffagnini, M., Morisse, S., Sparla, F., Perez-Perez, M.E., Francia, F. *et al.* (2013) Redox regulation of the Calvin-Benson cycle: Something old, something new. *Frontiers in Plant Science*, **4**, 470.

Mora-Garcia, S., Rodriguez-Suarez, R. & Wolosiuk, R.A. (1998) Role of electrostatic interactions on the affinity of thioredoxin for target proteins. Recognition of chloroplast fructose-1, 6-bisphosphatase by mutant *Escherichia coli* thioredoxins. *Journal of Biological Chemistry*, **273**, 16273–16280.

Morisse, S., Michelet, L., Bedhomme, M., Marchand, C.H., Calvaresi, M., Trost, P. *et al.* (2014) Thioredoxin-dependent redox regulation of chloroplastic phosphoglycerate kinase from *Chlamydomonas reinhardtii*. *Journal of Biological Chemistry*, **289**, 30012–30024.

Napolitano, S., Reber, R.J., Rubini, M. & Glockshuber, R. (2019) Functional analyses of ancestral thioredoxins provide insights into their evolutionary history. *Journal of Biological Chemistry*, **294**, 14105–14118.

Navrot, N., Gelhaye, E., Jacquot, J.P. & Rouhier, N. (2006) Identification of a new family of plant proteins loosely related to glutaredoxins with four CxxC motives. *Photosynthetic Research*, **89**, 71–79.

Nishizawa, A.N. & Buchanan, B.B. (1981) Enzyme regulation in C4 photosynthesis. Purification and properties of thioredoxin-linked fructose bisphosphatase and sedoheptulose bisphosphatase from corn leaves. *Journal of Biological Chemistry*, **256**, 6119–6126.

Ojeda, V., Perez-Ruiz, J.M. & Cejudo, F.J. (2018) 2-Cys peroxiredoxins participate in the oxidation of chloroplast enzymes in the dark. *Molecular Plant*, **11**, 1377–1388.

Okegawa, Y. & Motohashi, K. (2015) Chloroplastic thioredoxin m functions as a major regulator of Calvin cycle enzymes during photosynthesis in vivo. *Plant Journal*, **84**, 900–913.

Palde, P.B. & Carroll, K.S. (2015) A universal entropy-driven mechanism for thioredoxin-target recognition. *Proceedings of the National Academy of Sciences of the United States of America*, **112**, 7960–7965.

Pan, J.L. & Bardwell, J.C. (2006) The origami of thioredoxin-like folds. *Protein Science*, **15**, 2217–2227.

Perez-Perez, M.E., Mata-Cabana, A., Sanchez-Riego, A.M., Lindahl, M. & Florencio, F.J. (2009) A comprehensive analysis of the peroxiredoxin reduction system in the *Cyanobacterium synechocystis* sp. strain PCC 6803 reveals that all five peroxiredoxins are thioredoxin dependent. *Journal of Bacteriology*, **191**, 7477–7489.

Perez-Perez, M.E., Mauries, A., Maes, A., Tourasse, N.J., Hamon, M., Lemaire, S.D. *et al.* (2017) The deep thioredoxome in *Chlamydomonas reinhardtii*: New insights into redox regulation. *Molecular Plant*, **10**, 1107–1125.

Petoukhov, M.V., Franke, D., Shkumatov, A.V., Tria, G., Kikhney, A.G., Gajda, M. *et al.* (2012) New developments in the ATSAS program package for small-angle scattering data analysis. *Journal of Applied Crystallography*, **45**, 342–350.

Roos, G., Foloppe, N. & Messens, J. (2013) Understanding the pK(a) of redox cysteines: The key role of hydrogen bonding. *Antioxidants and Redox Signaling*, **18**, 94–127.

Schroter, Y., Steiner, S., Matthai, K. & Pfannschmidt, T. (2010) Analysis of oligomeric protein complexes in the chloroplast sub-proteome of nucleic acid-binding proteins from mustard reveals potential redox regulators of plastid gene expression. *Proteomics*, **10**, 2191–2204.

Schurmann, P. & Buchanan, B.B. (2008) The ferredoxin/thioredoxin system of oxygenic photosynthesis. *Antioxidants and Redox Signaling*, **10**, 1235–1274.

Setterdahl, A.T., Chivers, P.T., Hirasawa, M., Lemaire, S.D., Keryer, E., Miginiac-Maslow, M. *et al.* (2003) Effect of pH on the oxidation-reduction properties of thioredoxins. *Biochemistry*, **42**, 14877–14884.

Sevilla, F., Camejo, D., Ortiz-Espin, A., Calderon, A., Lazaro, J.J. & Jimenez, A. (2015) The thioredoxin/peroxiredoxin/sulfiredoxin system: Current overview on its redox function in plants and regulation by reactive oxygen and nitrogen species. *Journal of Experimental Botany*, **66**, 2945–2955.

Sun, J., Zheng, T., Yu, J., Wu, T., Wang, X., Chen, G. *et al.* (2017) TSV, a putative plastidic oxidoreductase, protects rice chloroplasts from cold stress during development by interacting with plastidic thioredoxin Z. *New Phytologist*, **215**, 240–255.

Tardif, M., Atteia, A., Specht, M., Cogne, G., Rolland, N., Brugiere, S. *et al.* (2012) PredAlgo: A new subcellular localization prediction tool dedicated to green algae. *Molecular Biology and Evolution*, **29**, 3625–3639.

Tarrago, L., Laugier, E., Zaffagnini, M., Marchand, C., Le Marechal, P., Rouhier, N. *et al.* (2009) Regeneration mechanisms of *Arabidopsis thaliana* methionine sulfoxide reductases B by glutaredoxins and thioredoxins. *Journal of Biological Chemistry*, **284**, 18963–18971.

Toledano, M.B., Delaunay-Moisan, A., Outten, C.E. & Igbaria, A. (2013) Functions and cellular compartmentation of the thioredoxin and glutathione pathways in yeast. *Antioxidants and Redox Signaling*, **18**, 1699–1711.

Trost, P., Fermani, S., Marri, L., Zaffagnini, M., Falini, G., Scagliarini, S. *et al.* (2006) Thioredoxin-dependent regulation of photosynthetic glyceraldehyde-3-phosphate dehydrogenase: Autonomous vs. CP12-dependent mechanisms. *Photosynthetic Research*, **89**, 263–275.

Vaseghi, M.J., Chibani, K., Telman, W., Liebthal, M.F., Gerken, M., Schnitzer, H. *et al.* (2018) The chloroplast 2-cysteine peroxiredoxin functions

© 2021 Society for Experimental Biology and John Wiley & Sons Ltd,

as thioredoxin oxidase in redox regulation of chloroplast metabolism. *Elife*, **7**.

Wang, Y., Wang, Y., Ren, Y., Duan, E., Zhu, X., Hao, Y. *et al.* (2020) White Panicle2 encoding thioredoxin z, regulates plastid RNA editing by interacting with multiple organellar RNA editing factors in rice. *New Phytologist*.

Watson, W.H., Pohl, J., Montfort, W.R., Stuchlik, O., Reed, M.S., Powis, G. *et al.* (2003) Redox potential of human thioredoxin 1 and identification of a second dithiol/disulfide motif. *Journal of Biological Chemistry*, **278**, 33408–33415.

Wedmann, R., Onderka, C., Wei, S., Szijarto, I.A., Miljkovic, J.L., Mitrovic, A. *et al.* (2016) Improved tag-switch method reveals that thioredoxin acts as depersulfidase and controls the intracellular levels of protein persulfidation. *Chemical Science*, **7**, 3414–3426.

Weichsel, A., Gasdaska, J.R., Powis, G. & Montfort, W.R. (1996) Crystal structures of reduced, oxidized, and mutated human thioredoxins: Evidence for a regulatory homodimer. *Structure*, **4**, 735–751.

Wimmelbacher, M. & Bornke, F. (2014) Redox activity of thioredoxin z and fructokinase-like protein 1 is dispensable for autotrophic growth of *Arabidopsis thaliana*. *Jouranl of Experimental Botany*, **65**, 2405–2413.

Wolosiuk, R.A. & Buchanan, B.B. (1978a) Activation of chloroplast NADP-linked glyceraldehyde-3-phosphate dehydrogenase by the ferredoxin/thioredoxin system. *Plant Physiology*, **61**, 669–671.

Wolosiuk, R.A. & Buchanan, B.B. (1978b) Regulation of chloroplast phosphoribulokinase by the ferredoxin/thioredoxin system. *Archives of Biochemistry and Biophysics*, **189**, 97–101.

Yokochi, Y., Sugiura, K., Takemura, K., Yoshida, K., Hara, S., Wakabayashi, K.I. *et al.* (2019) Impact of key residues within chloroplast thioredoxin-f on recognition for reduction and oxidation of target proteins. *Journal of Biological Chemistry*, **294**, 17437–17450.

Yoshida, K., Hara, A., Sugiura, K., Fukaya, Y. & Hisabori, T. (2018) Thioredoxin-like2/2-Cys peroxiredoxin redox cascade supports oxidative thiol modulation in chloroplasts. *Proceedings of the National Academy of Sciences of the United States of America*, **115**, E8296–E8304.

Yoshida, K. & Hisabori, T. (2016) Two distinct redox cascades cooperatively regulate chloroplast functions and sustain plant viability. *Proceedings of the National Academy of Sciences of the United States of America*, **113**, E3967–E3976.

Yoshida, K. & Hisabori, T. (2017) Distinct electron transfer from ferredoxin-thioredoxin reductase to multiple thioredoxin isoforms in chloroplasts. *Biochemical Journal*, **474**, 1347–1360.

Yoshida, K., Uchikoshi, E., Hara, S. & Hisabori, T. (2019a) Thioredoxin-like2/2-Cys peroxiredoxin redox cascade acts as oxidative activator of glucose-6-phosphate dehydrogenase in chloroplasts. *Biochemical Journal*, **476**, 1781–1790.

Yoshida, K., Yokochi, Y. & Hisabori, T. (2019b) New light on chloroplast redox regulation: Molecular mechanism of protein thiol oxidation. *Frontiers in Plant Science*, **10**, 1534.

Yua, Q.B., Ma, Q., Kong, M.M., Zhao, T.T., Zhang, X.L., Zhou, Q. *et al.* (2014) AtECB1/MRL7, a thioredoxin-like fold protein with disulfide reductase activity, regulates chloroplast gene expression and chloroplast biogenesis in *Arabidopsis thaliana*. *Molecular Plant*, **7**, 206–217.

Zaffagnini, M., De Mia, M., Morisse, S., Di Giacinto, N., Marchand, C.H., Maes, A. *et al.* (2016) Protein S-nitrosylation in photosynthetic organisms: A comprehensive overview with future perspectives. *Biochimica et Biophysica Acta*, **1864**, 952–966.

Zaffagnini, M., Fermani, S., Marchand, C.H., Costa, A., Sparla, F., Rouhier, N. *et al.* (2019) Redox homeostasis in photosynthetic organisms: Novel and established thiol-based molecular mechanisms. *Antioxidants and Redox Signaling*, **31**, 155–210.

© 2021 Society for Experimental Biology and John Wiley & Sons Ltd,